The structure of crystalline profilin–β-actin

Clarence E. Schutt*, James C. Myslik*, Michael D. Rozycki*, Nalin C. W. Goonesekere* & Uno Lindberg†

* Department of Chemistry, Henry H. Hoyt Laboratory, Princeton University, Princeton, New Jersey 08544, USA
† Department of Zoological Cell Biology, WGI, Arrhenius Laboratories for Natural Sciences, Stockholm University, S-10691 Stockholm, Sweden

The three-dimensional structure of bovine profilin–β-actin has been solved to 2.55 Å resolution by X-ray crystallography. There are several significant local changes in the structure of β-actin compared with α-actin as well as an overall 5° rotation between its two major domains. Actin molecules in the crystal are organized into ribbons through intermolecular contacts like those found in oligomeric protein assemblies. Profilin forms two extensive contacts with the actin ribbon, one of which appears to correspond to the solution contact *in vitro*.

THE discovery of myosin and filamentous actin (F-actin) in non-muscle cells intensified the search for mechanisms underlying force generation and movement in eukaryotic systems. This search led to the identification of proteins that interact with actin to modify its behaviour, forming a basis for the repertoire of structures and movements observed in non-muscle cells[1,2]. The presence of non-filamentous forms of actin in extracts of various non-muscle cells indicated that the control of filament assembly and disassembly may be a feature of the dynamic behaviour of cells[3,4].

The first hint that actin-binding proteins are important in controlling filament assembly came from the observation that binding of monomeric actin to DNase I inhibits both DNA hydrolysis and F-actin assembly[5]. Subsequently, the crystalline form of the DNase I inhibitor[6] was found to consist of non-muscle actin and a second actin-binding protein, profilin, in a 1:1 ratio[7,8]. Profilin inhibited the assembly of F-actin *in vitro* by sequestering monomeric actin[8], and evidence followed that the profilin-actin heterodimer is a cellular storage form of monomeric actin[9–11]. Thymosin β_4 is another component that controls F-actin assembly[12].

Profilin seems to link receptor-mediated transmembrane signalling and microfilament-based motility[13]. Hydrolysis of phosphatidylinositol (4,5)-bisphosphate ($PtdInsP_2$) by phospholipase $C_\gamma 1$ is inhibited by profilin, unless the enzyme has been activated by receptor kinase-dependent tyrosine phosphorylation[14,15]. Specific binding of $PtdInsP_2$ to profilin dissociates the profilin–actin complex[13,16,17]. Thus $PtdInsP_2$, appearing in the inner leaflet of the lipid bilayer of the plasma membrane as a result of transmembrane signalling, recruits profilin–actin to the site of filament assembly[15,17].

We report here the crystallographic determination (Table 1) of the bovine profilin–β-actin[18] structure at 2.55 Å resolution. X-ray amplitudes were phased with a combination of multiple isomorphous replacement and molecular replacement using the structure of α-actin[19] as a search model. This structure confirms the interpretation at low resolution that profilin–β-actin assembles into a higher-order structure in which actin molecules make extensive contacts across a 2_1 screw axis and profilin molecules intercalate between consecutive actin molecules lying along each edge of the actin 'ribbon'[20]. The actin–actin ribbon contact is more characteristic of an oligomeric protein contact than an incidental crystal contact. Considering that the profilin–β-actin crystal can be converted to a well diffracting, semicrystalline fibre under conditions known to dissociate the profilin–actin complex[20], the ribbon contact may be related to actin–actin contacts in F-actin, providing a starting point for constructing a model of the β-actin filament.

Comparison of β- and α-actins

The α-actin molecule is composed of two major domains, the smaller divided into subdomains 1 and 2, the larger divided into subdomains 3 and 4 (ref. 19). Bovine β-actin is generally similar in structure to α-actin, but a number of significant differences merit explanation. Alignment of α-carbon atoms in subdomain 3 (Fig. 2*a*), leads to superposition of a major portion of β-actin subdomain 4 onto α-actin, although local displacements of residues are observed at the top of subdomain 4 (residues 192–208 and 230–249, using the β-actin sequence of ref. 21) and the bottom of subdomain 3 (residues 275–291). A rotation of the small domain of β-actin relative to α-actin becomes apparent after this alignment. Most of subdomains 1 and 2 of β-actin can be superimposed onto α-actin after a torsion change of ($\Delta\phi = +5°$, $\Delta\psi = +2°$) at Ala 138, although residues 338–372 of β-actin are not moved in this operation and require a separate torsion change of ($\Delta\phi = -5°$, $\Delta\psi = +2°$) at Ser 338. Several stretches of residues are not superimposable by these torsion changes, including 2–5, 39–50 and 55–65. Normal mode analysis of monomeric α-actin predicted a similar hinging between the two domains in α-actin[22]. Hexokinase has been observed in two conformations related by rotations in a homologous region[23].

Differences in amino-acid conformations between the two actin isoforms fall into four categories. The first and second groups include residues whose main-chain atoms can be superimposed by one of the operations described, and whose resulting side-chain conformations are very similar, with only subtle differences in their interactions with neighbouring residues. Residues in the first group have side chains buried away from solvent, whereas those in the second group are partially or fully solvent-accessible. Residues that bind ATP fall into these two categories. As a result, the Sr^{2+}–ATP complex in β-actin lies in an environment similar to the Ca^{2+}–ATP complex in α-actin, and the cation–nucleotide complex itself adopts an almost identical conformation in the two isoforms. The third group consists of residues with significant changes in side-chain conformations. Residues in this group may project freely into solvent without interacting with other residues, or they accommodate different intermolecular contacts in the two crystals. For example, the phenol group of Tyr 169 in β-actin is rotated by 140° relative to its position in α-actin, allowing it to contact the side chain of Ile 73 on neighbouring profilin. The fourth group includes residues whose main-chain conformations are not superimposable by the operations described, leading to significantly changed side-chain orientations. Among the α/β sequence differences, residues Cys/Val 10, Val/Cys 17, Thr/Val 103, Val/Thr 129, Leu/Met 153, Asn/Thr 163, Thr/Ala 260, Asn/Thr 297 and Met/Leu 299 fall into the first group; Leu/Met 16, Ile/Val 76, Met/Leu 176, Asn/Thr 201, Ile/Leu 267, Ala/Cys 272, Tyr/Phe 279, Ile/Val 287, Thr/Ser 358 and Ala/Ser 365 are in the second group; Asn/Gln 225 is in the third group; and Glu/Asp 2, Glu/Asp 4, Thr/Ile 5 and Thr/Ala 6 fall in the fourth.

Several differences between the actin isoforms involve coordi-

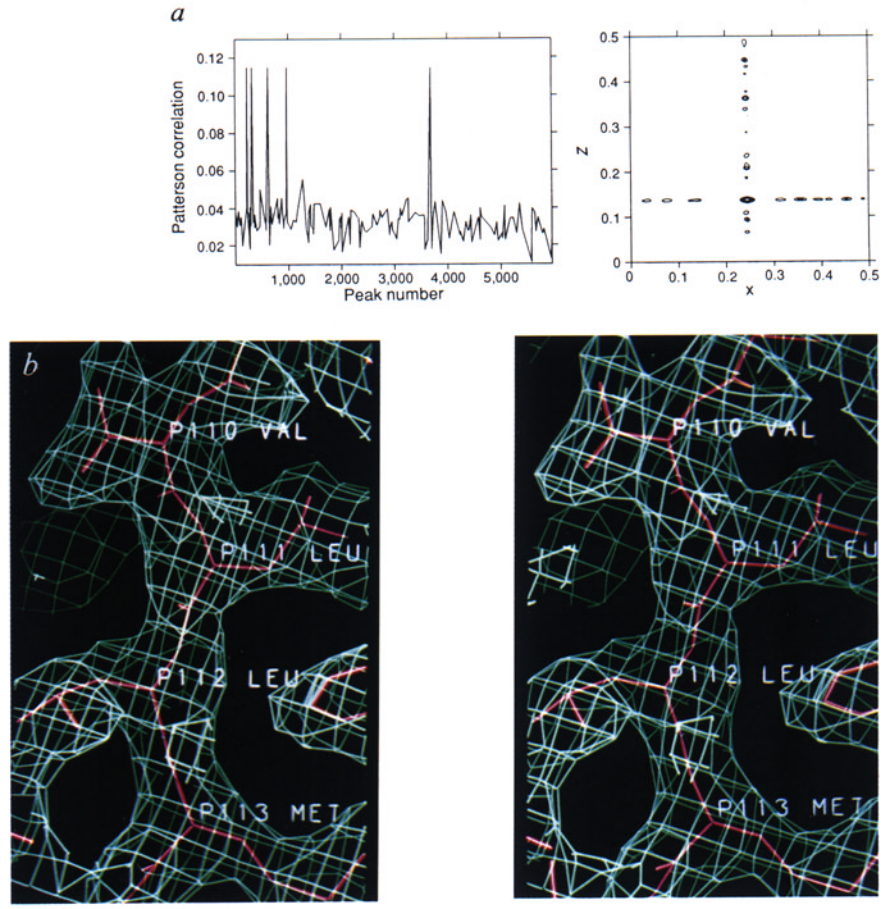

FIG. 1 Structure determination of bovine profilin–β-actin. *a*, Molecular replacement using a search model described in Table 1 legend. The search model was rotated and translated as a single, rigid unit using molecular replacement as implemented in X-PLOR[46]. The left-hand panel shows the refined Patterson correlation coefficients for the highest 6,000 rotation function solutions in the resolution range from 8.00 to 4.00 Å. The six highest peaks, one of which is occluded by the vertical axis, have Patterson correlation coefficients of 0.115 (4σ) and represent an equivalent unique solution at the pseudo-orthogonal eulerian angles of (75.2°, 72.9°, 84.4°). The right-hand panel gives the translation function calculated for the solution to the rotation function in the same resolution range. The plot is contoured from 5σ to maximum by σ, with the highest peak ($T=0.332$, 12σ) at ($x=0.219$, $y=0.247$, $z=0.140$). A full description of this procedure is presented in ref. 50. *b*, Portion of atomic model of profilin residues 110–113 (pink). The accompanying $2F_o-F_c$ omit map (green cage) was calculated after removal of an 8 Å radius sphere of the partially refined profilin–β-actin–ATP–Sr^{2+} model (Table 1 legend), centred at the α-carbon of profilin residue Leu 111, followed by simulated annealing refinement of the remainder of the model using X-PLOR. The map contouring level is 0.50σ.

nated changes in groups of residues. The first of these includes residues 37 and 52, which bind DNase I (ref. 19). Residues 37, 38 and 52 are nearly superimposable in the two isoforms, but residues deviate increasingly towards the middle of the loop. The side chains of Arg 37, Arg 39, Val 43, Met 44, Met 47 and Asp 51 show significant differences in orientation, which may be explained by the different crystalline environments of the isoforms. In α-actin, Gly 42, Val 43 and Met 44 form a β-strand that is incorporated into a β-sheet in DNase I (ref. 19), whereas in profilin–β-actin these residues form an actin–actin contact. Aspartic acid at position 51 forms a salt bridge with Arg 37 in β-actin which is not found in α-actin. This region appears to be one of relative mobility in β-actin, as evidenced by an average atomic temperature factor of 35 ± 3 Å^2 for these residues, compared with 20 Å^2 for the entire profilin–actin structure.

Structural differences in the amino-terminal region of actin are important because of its role in binding myosin and other actin-binding proteins[24]. Five α/β differences lie in the span of residues 1–6, including Asp 1, which is not present in β-actin[21]. This stretch is helical in α-actin. Substitution of Thr by Ile at residue 5 brings this residue closer to His 101 and Pro 102 in β-actin, causing a displacement relative to α-actin of Asp 2 through to Asp 4 (Fig. 2*b*) and a conformation change to a non-helical turn for these residues. Atomic temperature factors for residues 2–5 of β-actin average 33 ± 5 Å^2, indicating a relatively high positional uncertainty as found in α-actin[19].

Residues 373–375 of α-actin were removed before crystallization with DNase I (ref. 19). The local environment of these residues in crystalline profilin–β-actin is shown in Fig. 2*c*. The terminal α-helix starting at Ile 369 continues to Cys 374 in the β-actin structure with normal helical geometry. Lysine 373 extends underneath the helix to interact with Glu 361, while Cys 374 tucks into a pocket containing Tyr 133, Val 134 and Ile 357. The aromatic ring of Phe 375 is surrounded by hydrophobic side chains from Tyr 133, Ile 136, Val 139, Tyr 169, Ala 170 and Met 355. The carboxy terminus of β-actin has a stability comparable to the entire profilin–actin complex, as evidenced by average atomic temperature factors of 22 ± 5 Å^2 for residues 351–375, which may be due either to its interaction with profilin, described later, or to the presence of those residues missing in the α-actin crystal structure. Temperature factors above 40 Å^2 have been reported in this region for α-actin[19].

A difference between the two actin isoforms arises in the contact between the main body of subdomain 4 and the loop consisting of residues 264–273. In α-actin, the aromatic ring of Phe 266 lies in an energetically unfavourable environment next to the carboxylate group of Glu 259 (Fig. 2*d*). This instability has led Holmes *et al.* to propose that residues in this loop spontaneously refold in solution, forming a 'hydrophobic plug' which provides essential stabilization energy for their filament model[25]. In β-actin, the side-chain conformations of Phe 223 and Glu 259 are different, allowing for favourable interactions with the phenyl group of Phe 266 as well as a new electrostatic interaction of the carboxylate group of Glu 259 with Arg 312. This arrangement appears to stabilize the conformation of the 264–273 loop as it is found in the crystal. The average atomic temperature factor of 22 ± 5 Å^2 for residues 264–273 indicates relative stability for this region which may, however, derive from its proximity to a contact with profilin. Although three α/β sequence differences fall within this region (Ala 260, Leu 267 and Cys 272), they do not account for the differences because the two structures are superimposable in this region apart from the changes to Phe 223 and Glu 259 already described.

Profilin structure

Profilin is bisected by an antiparallel β-pleated sheet, as shown in Fig. 3*a*. Both termini are α-helical and pack against the same side of the central sheet, connecting to it by short loops. The

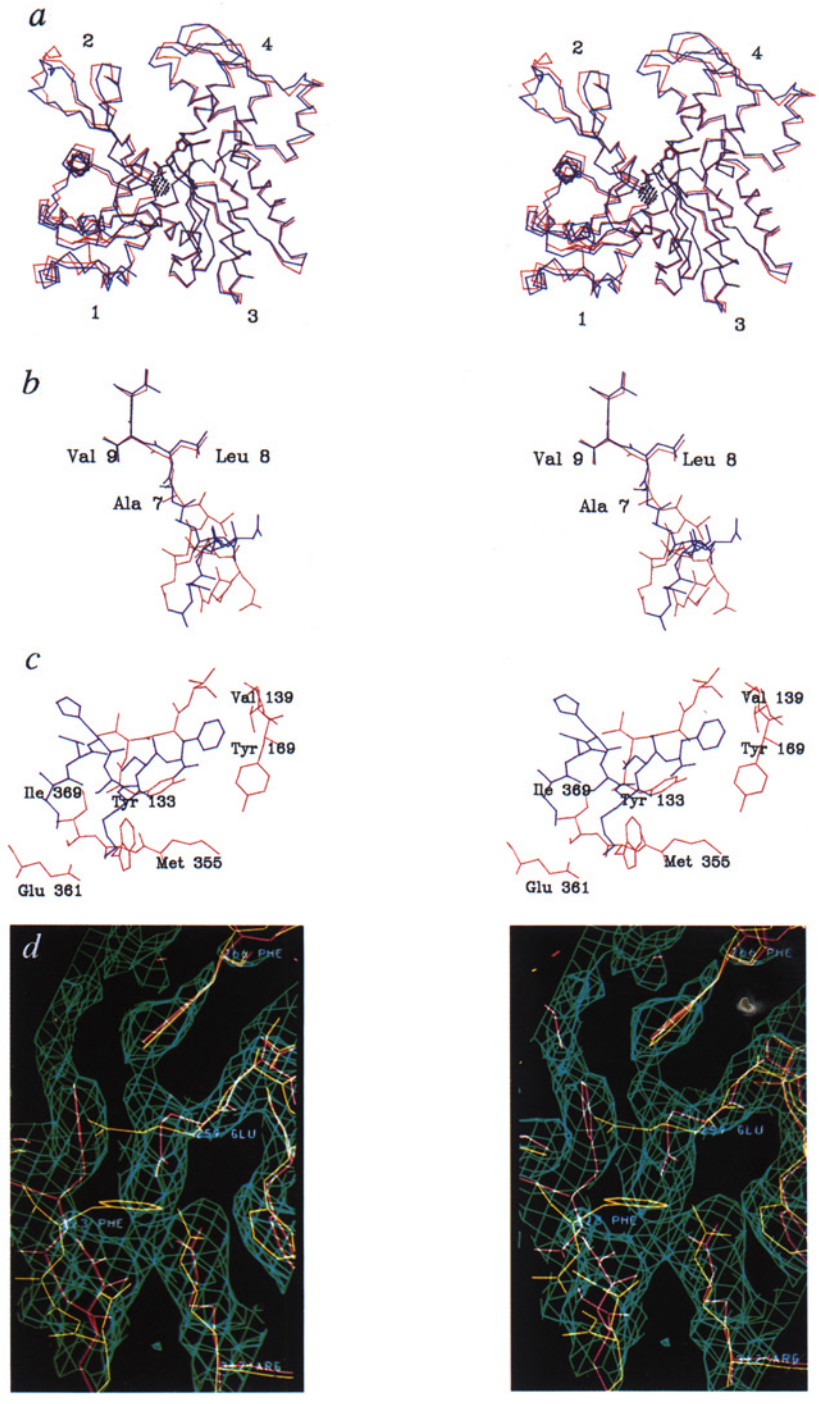

FIG. 2 Comparison of α- and β-actin. *a*, Comparison of α-carbon paths of β-actin (blue) and α-actin (red). The locations of the 4 subdomains are labelled according to ref. 19. Residues in subdomain 3 of the two isoforms were superimposed using a least-squares alignment of α-carbons for residues 135–182 and 263–335 using the program QUANTA (Polygen). The r.m.s. positional deviation of α-carbons for these residues was 0.497 Å. *b*, Comparison of the amino-terminal residues of β-actin (blue) and α-actin (red). Residues Ala 7, Leu 8, and Val 9 are labelled. The remaining residues shown in α-actin are Asp 1, Glu 2, Asp 3, Glu 4, Thr 5, Thr 6 and Cys 10, and in β-actin, Asp 2, Asp 3, Asp 4, Ile 5, Ala 6 and Val 10. *c*, Carboxy terminus of β-actin. Residues 369–375 are shown in blue, residues Tyr 133, Val 134, Ala 135, Ile 136, Val 139, Tyr 169, Ala 170, Met 355, Trp 356, Ile 357 and Glu 361 are shown in red. The amino-terminal residue is labelled in each fragment. *d*, Comparison of side-chain orientations of Phe 223, Asp 259, Phe 266 and Arg 312 in β-actin (pink) and α-actin (yellow). Accompanying $2F_o - F_c$ omit map (green cage) was calculated after omission of an 9 Å-radius model sphere, centred at the α-carbon of β-actin residue Phe 223, and simulated annealing refinement of the remainder of the model using X-PLOR (see Table 1 legend). The map contouring level is 0.50σ.

amino-terminal helix (H1) packs flat against strands 1, 2 and 7, and the carboxy-terminal helix (H4) lies next to it against strands 5, 6 and 7. The two helices do not pack tightly against each other, but contribute side chains to a common hydrophobic core involving the β-sheet, as well as to a salt bridge between Asp 8 and Lys 126. Residues on the opposing face of the central sheet contribute to a second, more extensive hydrophobic core populated by aliphatic residues and bounded by two small α-helices (H2 and H3) and a short β-hairpin containing strands 3 and 4. This latter core is sealed from above by the loop connecting strands 1 and 2, and at the side by a helical turn preceding helix 2. A β-bulge at Ile 73 redirects strand 4, bending it into the central sheet. This bend is stabilized by an interaction between Arg 55 and Asp 75. Strands 5 and 6 are connected by a type-II turn and form a protrusion from the profilin surface. The polypeptide fold of strands 3 to 6 of bovine profilin is similar to those found for several SH3 domains[26].

Alignment of 16 profilin sequences in the Swiss Protein Database showed that residues Trp 3, Tyr 6, Trp 31 and Leu 134 are strictly invariant, except in the putative profilin sequence from the virus vaccinia (Table 2); His 133 and Tyr 139 are also highly conserved in these sequences. These residues lie on a solvent-exposed surface between helix 1 and helix 4 (Fig. 3*b*). A second extensive, but less strongly conserved, hydrophobic surface patch contains residues Tyr 24, Pro 28, Pro 44, Val 51, Leu 78, Phe 83, Met 104, Ala 106, Tyr 128 and Arg 135.

Protein–protein interactions

The extensive crystal contact between α-actin and DNase I enabled a correspondence between the crystalline and solution

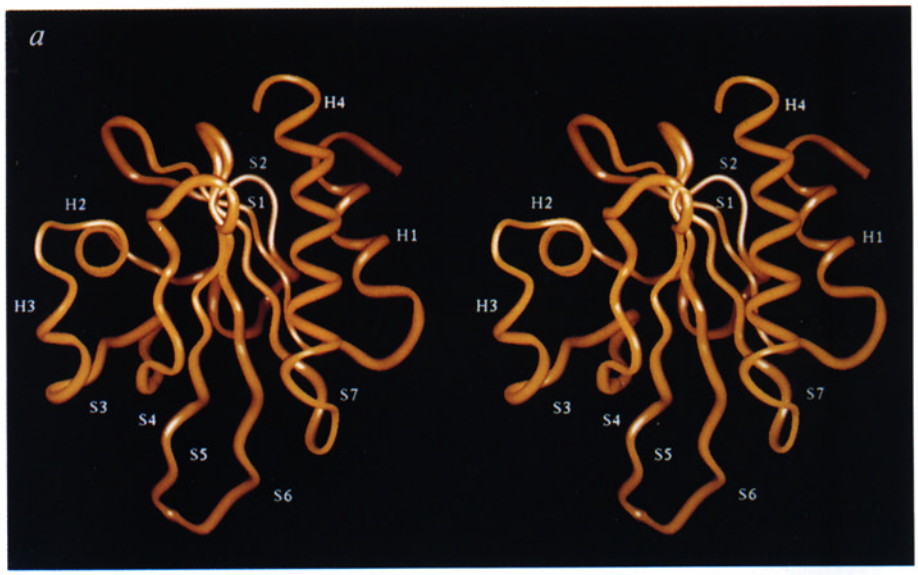

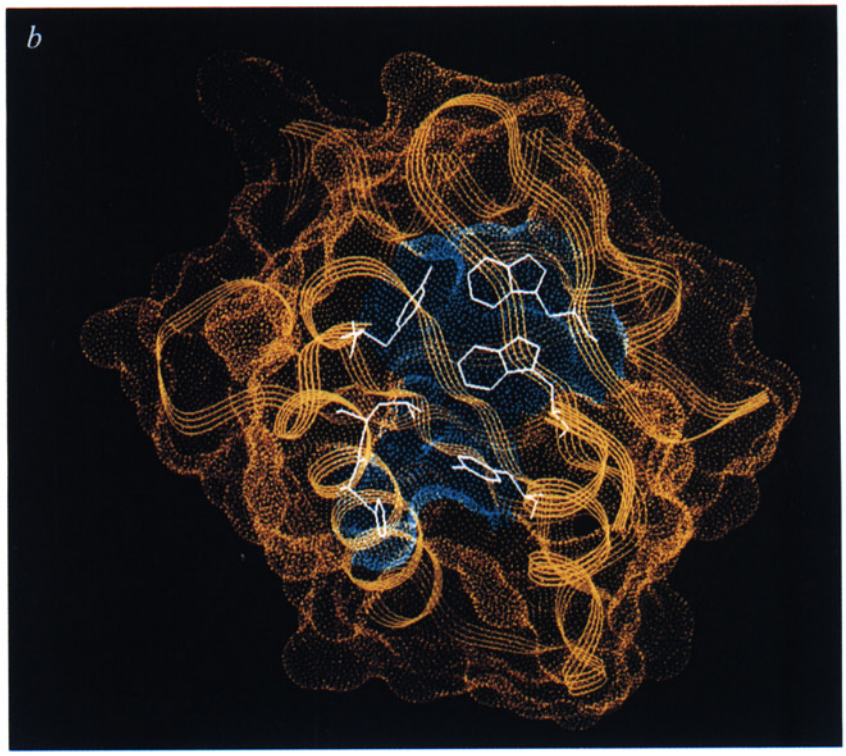

FIG. 3 Structure of bovine profilin. *a*, Polypeptide fold of profilin. Labelled elements of secondary structure include helix 1 (H1), residues 2–11; helix 2 (H2), 44–51; helix 3 (H3), 57–61; helix 4 (H4), 120–136; strand 1 (S1), 17–24; strand 2 (S2), 32–34; strand 3 (S3), 62–64; strand 4 (S4), 69–76; strand 5 (S5), 83–90; strand 6 (S6), 97–104 and strand 7 (S7), 109–114. *b*, Highly conserved hydrophobic residues in profilin form a solvent-exposed hydrophobic surface. The polypeptide fold of profilin is depicted as a yellow ribbon. Residues in white are (clockwise from top right) Trp 31, Trp 3, Tyr 6, His 133, Leu 134 and Tyr 139. Solvent-exposed surfaces are depicted for these residues by blue–green dots and for the remainder of profilin in brown dots. The probe radius for solvent-exposed surfaces was 1.40 Å.

binding sites of DNase I and α-actin to be established[19]. We expected a similar result for crystalline profilin–β-actin and considered it likely that profilin, in view of its proposed function as a monomer-sequestering protein, would bind to β-actin to block the actin–actin contacts in filaments. But analysis of low-resolution electron density maps revealed that both profilin–β-actin and β-actin–β-actin contacts are extensive in the crystalline state[20]. The present high-resolution structure confirms this view by verifying the molecular boundaries and enabling intermolecular contacts to be evaluated.

The high-resolution structure of profilin–β-actin is presented in Fig. 4*a*. Profilin forms two major contacts with actin in the crystal. The primary contact comprises a region of profilin defined by helix 3, the amino-terminal portion of helix 4, and strands 4, 5 and 6. This region makes contact with a site on actin spanning the large and the small domains of the molecule at the bases of subdomains 1 and 3. Formation of this contact buries a combined interfacial surface area on profilin and actin of 2,250 Å^2. Twenty-one residues each from actin and profilin contribute to this contact (Fig. 4*b*), resulting in a close-packed, complementary surface of ionic, polar and hydrophobic interactions, including ten hydrogen bonds. The buried surface area of this contact is approximately ten times that of a typical protein:protein crystal contact and lies in the range observed for functionally important protein interfaces such as those found in protease–inhibitor and antibody–antigen complexes[27]. For comparison, the crystal contact which has been identified as the solution binding site between DNase I and α-actin[19] buries a combined area of 1,830 Å^2 between the two proteins.

Biochemical studies indicate that the primary profilin–actin contact corresponds to the contact observed in solution. Removal of Phe 375 from β-actin by carboxypeptidase A digestion decreases the stability of the profilin–actin complex[28]. This finding is consistent with the central role of Phe 375 in this contact; the phenyl ring interacts with Ile 73, His 119, Gly 121 and Asn 124 of profilin, while the terminal carboxylate group forms

a salt bridge with Arg 74 of profilin. A second observation is that Lys 125 of profilin and Glu 364 of actin form an intermolecular electrostatic interaction at the profilin–actin contact site. Glutamate 364 of actin has been chemically crosslinked to Lys 115 of profilin from *Acanthamoeba castellani*[29], which in sequence alignment is homologous to Lys 125 of bovine profilin. Finally, profilin–actin dissociates when the pH is less than 6.0 (ref. 30) suggesting that histidyl residues are involved in the intermolecular contact. The profilin–actin contact at subdomains 1 and 3 of actin is the only contact involving histidyl residues; the imidazole ring His 173 of actin stacks upon the phenyl ring of Phe 59 of profilin and His 119 of profilin sits in a pocket formed by Tyr 169, Met 355 and Phe 375 of actin. Protonation of these residues leading to formation of positively charged imidazolium ions would destabilize these apolar interactions.

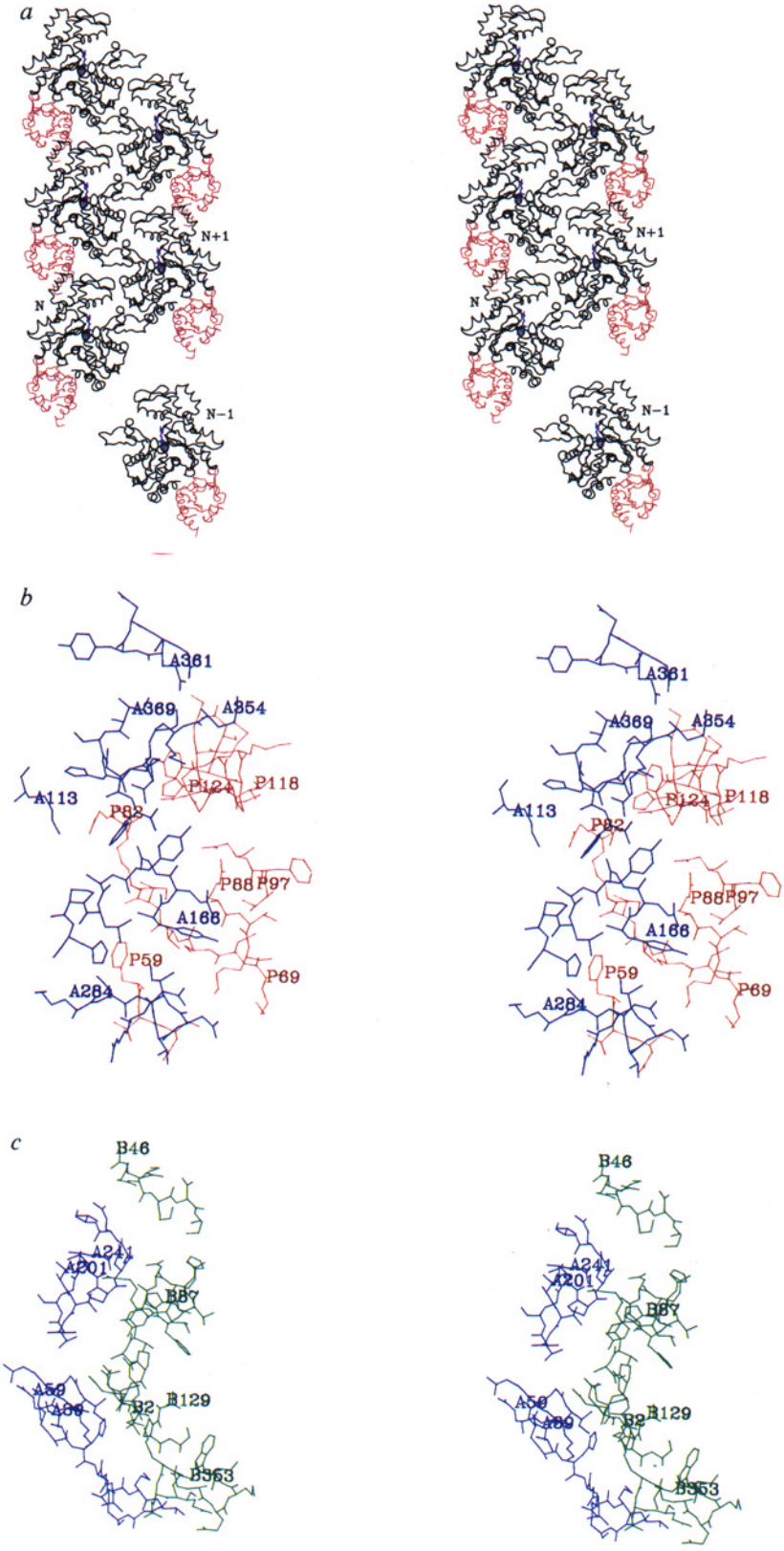

FIG. 4 Organization of profilin and actin in profilin–β-actin crystals. *a*, The profilin–actin ribbon. Actin and profilin are depicted in black and red, respectively. ATP is shown as a blue stick figure, and Sr^{2+} as a blue sphere at the van der Waals radius. Five profilin–actin heterodimers are shown in an intact ribbon. The *n*th monomer lying at the bottom of the ribbon makes an extensive contact with monomer $n+1$ lying across a 2_1 screw axis lying in the plane of the page parallel to the long axis of the ribbon. A sixth heterodimer $(n-1)$ is shown removed from the ribbon to show the solution complex. *b*, The primary profilin–actin contact. Amino-terminal residues only are labelled in each fragment except for P124 which has been labelled for orientation. Actin and profilin are in blue and red, respectively. The contact can be divided into two parts. The first involves contacts between Glu 82, Val 118, His 119, Gly 121, Met 122, Asn 124, Lys 125, Tyr 128 and Glu 129 of profilin and residues of β-actin subdomain 1 including Lys 113, Gln 354, Met 355, Glu 361, Glu 364, Ile 369, His 371, Arg 372, Lys 373 and Phe 375. The second part includes profilin residues Phe 59, Val 60, Asn 61, Lys 69, Ser 71, Val 72, Ile 73, Arg 74, Arg 88, Lys 90, Thr 97 and Asn 99, and β-actin subdomain 3 residues Tyr 166, Glu 167, Tyr 169, Leu 171, Pro 172, His 173, Lys 284, Asp 286, Val 287, Asp 288 and Arg 290. Total buried surface area was calculated according to ref. 51 using X-PLOR. The probe radius was 1.4 Å. A residue was considered to participate in a contact if its solvent-accessible surface area in the isolated monomer decreased by 10 $Å^2$ or more in forming the interaction. The criteria for hydrogen bonding were (1) a distance between donor and acceptor atoms no greater than 3.4 Å, and (2) an angle of 110° or more between donor atom, acceptor atom and antecedent. *c*, The actin–actin ribbon contact. Only amino-terminal residues are labelled in each fragment. The actin molecule drawn in green (molecule B) is related to the one drawn in blue (molecule A) by the operation of a 2_1-screw axis parallel to the crystallographic *b*-axis. The interface can be dissected into two subcontacts. At the bottom of the figure, the small domain of molecule A (His 40, Gln 41, Gly 42, Met 44, Val 45, Gly 46, Ser 60, Lys 61, Gly 63 and Ile 64) makes contact with the small domain of molecule B (acetyl-Asp 2, Asp 4, Asp 5, Glu 99, Glu 100, Pro 130, Ala 131, Gln 353, Ser 358 and Gln 360). At the top, the large domain of molecule A (Thr 202, Ala 204, Gly 205, Pro 243, Asp 244, Gly 245, Gln 246 and Val 247) makes contact with the small domain of molecule B (Gly 48, Lys 50, His 87, Tyr 91, Asn 92, Arg 95 and Ala 97). Both of the subcontacts are predominantly apolar except for the side chains of His 40 and Asp 2, and Glu 205 and Arg 95. Total buried surface area was calculated as in *b*.

Each actin molecule in crystalline profilin–β-actin makes contact with eight other actin molecules[20]. The most extensive contact is made between two actin molecules related to one another by a 2_1 screw axis parallel to the crystallographic *b*-axis, giving rise to the zig-zag ribbon structure shown in Fig. 4*a*. The interface at this 'ribbon contact' buries 1,670 Å^2 of total surface area between the two monomers involved. By comparison, the most extensive actin–actin contact in the DNase I–α-actin crystal buries a combined surface area of only 150 Å^2. Seventeen residues are contributed from each protein at the ribbon contact. No hydrogen bonds are found at this contact. Instead, hydrophobic interactions predominate (Fig. 4*c*), even for residues containing charged groups. Exceptions to this are the Arg 95 : Glu 205 and His 40 : Asp 2 interactions. The ribbon contact is comparable in extent to the primary profilin–β-actin and DNase I/α-actin contacts, and is significantly larger than contacts found typically in crystals. As with the primary profilin–actin contact, it lies in the range observed for known protein interfaces, although the close packing of predominantly hydrophobic groups is more characteristic of oligomeric protein contacts than of protease–inhibitor or antibody–antigen complexes[27,31].

TABLE 1 Crystallographic analysis

	Native	K_2OsO_4	K_2PtCl_4
Resolution (Å)	2.55	2.55	2.55
Unique reflections	16,158	15,160	15,156
Completeness (%)	98.8	92.7	92.7
R^*_{sym} (*I*) (%) ($I > 0$)	6.5	7.1	7.3

Refinement (8.0–2.55 Å)

Resolution range (Å)	Reflections/completeness ($\|F\| > 3\sigma\|F\|$)/(%)	*R*-factor (%)	$R^\dagger_{cum}$ (%)
4.76–8.00	1,949/94	19.35	19.35
3.92–4.76	1,968/98	15.06	17.07
3.47–3.92	1,946/97	17.65	17.24
3.18–3.47	1,877/98	19.80	17.70
2.96–3.18	1,836/96	21.83	18.21
2.80–2.96	1,732/94	25.82	18.90
2.66–2.80	1,688/83	27.67	19.50
2.55–2.66	1,539/82	29.61	20.05

r.m.s. deviation, bond length	0.018 Å
r.m.s. deviation, bond angle	3.84°
Overall restrained B-factor	19.9 Å^2

Calf spleen profilin–β-actin was purified and crystallized as described[6,7,18]. X-ray film data was processed as described for native and derivatized crystals[44]. Crystallographic analysis was carried out using the CCP4 program suite[45]. Multiple isomorphous replacement (MIR) phases were obtained to better than 2.6 Å and are described in detail in ref. 20; however, only K_2OsO_4 and K_2PtCl_4 derivatives were used here. The MIR electron density map contained elements of recognizable secondary structure but sufficient ambiguities remained in connecting regions that sequence assignment could not be completed without additional phase information from molecular replacement (MR). A search model was used containing amino-acid residues 7–38 and 52–348 of α-actin, without nucleotide or divalent cation. Remaining residues were omitted because of high-temperature factors at the termini[19] and because structural changes were anticipated at the DNase I-binding site. The search model was rotated and translated in the profilin–β-actin unit cell using the macromolecular analysis program X-PLOR (version 3.0)[46]. A solution was obtained for the unique alignment of the model with β-actin (Fig. 1*a*). Rotational and translational searches were made for the four individual subdomains of α-actin, and solution positions were nearly identical to those for the intact molecule. Residues in β-actin which differ from α-actin[21] were substituted into the MR solution, and Sr^{2+}–ATP, used for profilin–β-actin crystallization[20], was fit to the electron density. The resulting starting model for β-actin was refined by conjugate-gradient minimization in X-PLOR using native X-ray amplitudes between 10.0 and 3.4 Å. Phases calculated from this refined model and amplitudes from native and OsO_4^{2-}-derivative data were used to calculate difference Fourier transforms which gave peaks at the previously identified[20] OsO_4^{2-} sites in the unit cell. Simulated annealing at this point led to degradation of phase quality observed as increase in noise in the difference Fourier, an effect that was not evident after completion of model building. Model phases were combined with MIR phases and an electron density map calculated. Residues 2–6, 39–40 and 349–375 of β-actin (numbered according to ref. 21) were modelled using FRODO[47], augmented with the structural database searching program FRAGLE[48]. An initial model for roughly half of the 139 residues of profilin was made by building secondary structural elements and connecting loops as polyalanine fragments. A new phase-combined map was calculated adding the newly modelled fragments of actin and profilin to the first model. This map showed sufficient continuity and side-chain density to model the amino-acid sequence[49] of bovine profilin. The resulting profilin–β-actin model was completed apart from residues 41 to 51 of β-actin and 138 and 139 of profilin, which were still difficult to fit to electron density. The model was refined by simulated annealing from 3,000 K in X-PLOR between 8.0 and 2.6 Å. Independence of the refined model from the α-actin search model was evaluated by examining each residue for fit to an 'omit map'. Profilin residues (1–137) and residues 6–35, 70–135, 335–375 of actin constituted a half-model which was divided into overlapping spheres of radii 7–9 Å. For each sphere, an annealed omit map[46] was calculated between 6.00 and 2.60 Å. Residues within each sphere were examined for agreement to electron density in the map and adjusted as necessary to improve their fit. Phases from the adjusted half-model were combined with MIR phases to produce another map. The remaining residues in β-actin were examined in this map, including the Sr^{2+}–ATP complex, and the previously unfit residues 41–51 of actin and 138–139 of profilin were inserted. The completed profilin–β-actin–Sr^{2+}–ATP model was refined between 8.00 and 2.55 Å in X-PLOR using simulated annealing followed by restrained refinement of atomic temperature factors. Coordinates of the complex will be deposited in the Brookhaven Protein Database.

* $R_{sym} = \Sigma |I - \langle I \rangle| / \Sigma I$, where *I* is the intensity of a given reflection, and $\langle I \rangle$ is the mean intensity of symmetry-related reflections.

† R_{cum} is the cumulative *R*-factor.

In addition, profilin forms a contact with a second actin molecule, fitting the amino-terminal helix of profilin into a groove formed by three of the four helices of subdomain 4. Thus profilin appears to act as a wedge between adjacent actin molecules, stabilizing the ATP-containing ribbon in the crystal (Fig. 4*a*). This second profilin-actin interaction buries 1,110 Å^2 of combined interfacial area, contributed by 14 residues from actin and 11 from profilin. Only one hydrogen bond is found, and the interactions at this site are mainly hydrophobic. These characteristics are more like the actin–actin ribbon contact than the primary profilin–actin contact.

Implications of the ribbon structure

Actin functions as a self-assembling protein, and the ribbon contact may be related to the actin–actin contacts in actin filaments. It is not unusual for protein crystals and fibres to use similar intermolecular contacts. Crystallization of sickle deoxyhaemoglobin S (HbS) seems to compete with formation of 14-strand fibres[32]. Within the resolution limits of electron microscopy and fibre diffraction, it appears that both processes incorporate the same basic functional unit, a ribbon of two half-staggered strands of HbS tetramers[32]. The combined buried interfacial surface area between contacts within HbS ribbons (880 Å^2 for the lateral, 890 Å^2 for the axial tetramer contacts) are comparable to the actin–actin contacts in the profilin–β-actin ribbons. In the bacterial RecA protein, crystal contacts have been used to model the inactive form of the RecA filament[33].

On the basis of two observations, we have proposed that the actin ribbon represents a twisted and stretched form of filamentous actin stabilized by profilin[20]. First, assembly of paracrystalline F-actin competes with crystal growth in solution and, by analogy with HbS, may use closely related actin–actin contacts[20]. Second, the profilin–β-actin crystal lattice can be converted to a well diffracting, semi-crystalline fibre after transfer to low pH[20], which dissociates profilin from actin[30]. In addition, three-dimensional reconstructions of F-actin imaged by cryo-electron microscopy show a striking resemblance between the wide view of the filament and the profilin–actin ribbon[34]. The present high-resolution structure extends our previous studies on the actin ribbon by providing evidence for a specific oligomeric interaction. The footprint of one actin molecule on its neighbour in the ribbon includes a region of the sequence that is nearly identical to that associated with the DNase I–α actin contact. DNase I binds both the small and large domains of actin at subdomains 2 (residues 39–46, 60–64) and 4 (residues 202–204 and 207)[19]. Thus DNase I, which inhibits filament assembly, contacts all of the residues in subdomain 2 and two of the seven residues in subdomain 4 that are involved in the ribbon contact.

The role of profilin

Compared with α-actin, β-actin as it appears in the profilin–

TABLE 2 Conservation of solvent-exposed hydrophobic residues in profilin

	Residue (aligned with bovine sequence)					
Bovine	W3	Y6	W31	H133	L134	Y139
Human	W	Y	W	H	L	Y
Mouse	W	Y	W	H	L	Y
White birch	W	Y	W	Y	L	L
Sea urchin	W	Y	W	Y	L	M
Sand dollar	W	Y	W	Y	L	M
Drosophila	W	Y	W	Y	L	Y
Physarum I	W	Y	W	Y	L	Y
Physarum II	W	Y	W	Y	L	Y
Tetrahymena	W	Y	W	T	L	Y
Dictyostelium I	W	Y	W	Y	L	Y
Dictyostelium II	W	Y	W	Y	L	C
Acanthamoeba I	W	Y	W	Y	L	F
Acanthamoeba II	W	Y	W	Y	L	F
Saccharomyces	W	Y	W	Y	L	Y
Vaccinia virus	W	I	L	R	V	N

actin ribbon has a 5° rotation between its two major domains. This rotation could be invoked to account for the increased rate of nucleotide exchange on actin in the presence of profilin[35]. However, the structural similarity between the nucleotide-binding sites in the two actin isoforms argues against this explanation. Furthermore, it is possible that the domain rotation represents the native structure of β-actin or a conformation induced during formation of the ribbon contact.

It is surprising that neither of the two contacts between profilin and actin use the conserved hydrophobic surfaces of profilin. The more highly conserved surface shown in Fig. 3*b* lies between the two terminal helices that bind actin, suggesting that these residues have a regulatory role. The specific affinity of profilin for poly(L-proline)[36] is abolished by mutagenesis of two of the residues in this region (Trp 3 or His 133)[37]. SH3 domains bind proline-rich sequences downstream of receptor-linked tyrosine kinases[38], and the similarities between bovine profilin and SH3 domains suggest that they carry out related docking functions in signalling pathways. The ability of profilin to bind simultaneously to actin ribbons and proline-rich sequences could serve an important function in actin-based motility. For example, this could explain the role of profilin in establishing links between growing actin filaments and the bacterial protein Act A at the tail of *Listeria monocytogenes*[39], providing propulsion for bacterial cells through the eukaryotic cytoplasm[40].

A second role for the conserved hydrophobic surface shown in Fig. 3*b* is suggested by the fluorescence quenching of Trp 3 and Trp 31 in the presence of $PtdInsP_2$ (ref. 41). These residues lie adjacent to a proposed $PtdInsP_2$ binding sequence[42] on helix 4. If fatty acid chains of $PtdInsP_2$ bind the hydrophobic surface, the four positively charged residues in helix 4 (Lys 125, Lys 126, Arg 135 and Arg 136) could bind the phosphoinositol head group, accounting for the ability of $PtdInsP_2$ to dissociate bovine profilin–actin *in vitro*[13]. But as micellar $PtdInsP_2$ binding to profilin was used, further investigation is necessary to determine whether a single-molecule binding site for $PtdInsP_2$ exists on profilin.

Discussion

Our crystallographic analysis presents an atomic-resolution view of the profilin–β-actin ribbon as a discrete structural entity. Model building, constrained by diffraction data and augmented by biophysical studies of mutated actin molecules[43], will help to establish whether the actin–actin contacts in the ribbon are related to those in F-actin. Profilin serves as a molecular wedge between actin molecules in the ribbon, apparently binding two complementary sites on actin. The ability of profilin to bind two actin molecules suggests that profilin serves a more intricate role in regulating actin than serving simply as a monomer-sequestering protein. □

Received 11 June; accepted 24 September 1993.

1. Stossel, T. B. *et al. A. Rev. Cell Biol.* **1,** 353–402 (1985).
2. Pollard, T. D. & Cooper, J. A. *A. Rev. Biochem.* **55,** 987–1035 (1986).
3. Probst, E. & Lüscher, F. *Biochim. biophys. Acta* **278,** 577–584 (1972).
4. Bray, D. & Thomas, C. *J. molec. Biol.* **105,** 527–544 (1976).
5. Lazarides, E. & Lindberg, U. *Proc. natn. Acad. Sci. U.S.A.* **71,** 4742–4746 (1974).
6. Lindberg, U. *J. biol. Chem.* **241,** 1246–1248 (1966).
7. Carlsson, L. *et al. J. molec. Biol.* **105,** 353–366 (1976).
8. Carlsson, L., Nyström, L.-E., Sundkvist, I., Markey, F. & Lindberg, U. *J. molec. Biol.* **115,** 465–483 (1977).
9. Markey, F., Persson, T. & Lindberg, U. *Cell* **23,** 145–153 (1981).
10. Southwick, F. S. & Young, C. L. *J. Cell Biol.* **110,** 1965–1973 (1990).
11. Tilney, L. G., Bonder, E. M., Coluccio, L. M. & Mooseker, M. S. *J. Cell Biol.* **97,** 112–124 (1983).
12. Safer, D., Golla, R. & Nachmias, V. T. *Proc. natn. Acad. Sci. U.S.A.* **87,** 2536–2540 (1990).
13. Lassing, I. & Lindberg, U. *Nature* **314,** 472–474 (1985).
14. Goldschmidt-Clermont, P. J., Machesky, L. M., Baldassare, J. J. & Pollard, T. D. *Science* **247,** 1575–1577 (1990).
15. Goldschmidt-Clermont, P. J., Kim, J. W., Machesky, L. M., Rhee, S. G. & Pollard, T. D. *Science* **251,** 1231–1233 (1991).
16. Lassing, I. & Lindberg, U. *J. cell. Biochem.* **37,** 255–267 (1988).
17. Lassing, I. & Lindberg, U. *Expl Cell Res.* **174,** 1–15 (1988).
18. Segura, M. & Lindberg, U. *J. biol. Chem.* **259,** 3949–3954 (1984).
19. Kabsch, W., Mannherz, H. G., Suck, D., Pai, E. F. & Holmes, K. C. *Nature* **347,** 37–44 (1990).
20. Schutt, C. E., Lindberg, U., Myslik, J. & Strauss, N. *J. molec. Biol.* **209,** 735–746 (1989).
21. Vandekerckhove, J. S. & Weber, K. *Eur. J. Biochem.* **90,** 451–462 (1978).
22. Tirion, M. T. & ben-Avraham, D. *J. molec. Biol.* **230,** 186–195 (1993).
23. Bennett, W. S. & Steitz, T. A. *J. molec. Biol.* **140,** 211–223 (1980).
24. Vandekerckhove, J. *Curr. Opin. Cell Biol.* **2,** 41–50 (1990).
25. Holmes, K. C., Popp, D., Gebhard, W. & Kabsch, W. *Nature* **347,** 44–49 (1990).
26. Noble, M. E. M., Musacchio, A., Saraste, M., Courtneidge, S. A. & Wierenga, R. K. *EMBO J.* **12,** 2617–2624 (1993).
27. Janin, J. & Chothia, C. *J. biol. Chem.* **265,** 16027–16030 (1990).
28. Malm, B., Larsson, H. & Lindberg, U. *J. Muscle Res. Cell Motil.* **4,** 569–588 (1983).
29. Vandekerckhove, J. S., Kaiser, D. A. & Pollard, T. D. *J. Cell Biol.* **109,** 619–626 (1989).
30. Carlsson, L. thesis Uppsala Univ., Sweden (1979).
31. Janin, J., Miller, S. & Chothia, C. *J. molec. Biol.* **204,** 155–164 (1988).
32. Rodgers, D. W., Crepeau, R. H. & Edelstein, S. J. *Proc. natn. Acad. Sci. U.S.A.* **84,** 6157–6161 (1987).
33. Story, R. M., Weber, I. T. & Steitz, T. A. *Nature* **355,** 318–325 (1992).
34. Milligan, R. A., Whittaker, M. & Safer, D. *Nature* **348,** 217–221 (1990).
35. Goldschmidt-Clermont, P. J., Machesky, L. M., Doberstein, S. K. & Pollard, T. D. *J. Cell Biol.* **113,** 1081–1089 (1991).
36. Tanaka, M. & Shibata, H. *Eur. J. Biochem.* **151,** 291–297 (1985).
37. Björkegren, C., Rozycki, M., Schutt, C., Lindberg, U. & Karlsson, R. *FEBS Lett.* (in the press).
38. Ren, R., Mayer, B. J., Cicchetti, P. & Baltimore, D. *Science* **259,** 1157–1161 (1993).
39. Kocks, Ç. *et al. Cell* **68,** 521–531 (1992).
40. Theriot, J. A., Mitchison, T. J., Tilney, L. G. & Portnoy, D. A. *Nature* **357,** 257–260 (1992).
41. Raghunathan, V., Mowery, P., Rozycki, M., Lindberg, U. & Schutt, C. *FEBS Lett.* **297,** 46–50 (1992).
42. Yu, F.-X., Sun, H.-Q., Janmey, P. A. & Yin, H. L. *J. biol. Chem.* **267,** 14616–14621 (1992).
43. Aspenström, P., Schutt, C. E., Lindberg, U. & Karlsson, R. *FEBS Lett.* **329,** 163–170 (1993).
44. Winkler, F. K., Schutt, C. E. & Harrison, S. C. *Acta crystallogr.* A**35,** 901–911 (1979).
45. CCP4 Package (Daresbury Laboratory, UK. 1979).
46. Brünger, A. T. *X-PLOR v. 3.0 manual.* (Yale Univ., New Haven, 1992).
47. Jones, T. A. *J. appl. Crystallogr.* **11,** 268–272 (1978).
48. Finzel, B. C. *et al.* in *Crystallographic Modelling Methods in Molecular Design* (eds Bugg, C. E. & Ealick, S. E.) 175–188 (Springer, New York, 1990).
49. Ampe, C., Markey, F., Lindberg, U. & Vandekerckove, J. *FEBS Lett.* **228,** 17–21 (1988).
50. Myslik, J. C. thesis, Princeton Univ., USA (1992).
51. Lee, B. & Richards, F. M. *J. molec. Biol.* **55,** 379–400 (1971).

ACKNOWLEDGEMENTS. We thank W. Kabsch and K. Holmes for providing us with the atomic coordinates of α-actin before their deposition in the Brookhaven Protein Database and T. Twomey and E. Girit for technical assistance. This work was supported by grants to C.E.S. from the National Institutes of Health, Carter-Wallace Inc. and Sterling-Winthrop Pharmaceuticals, and to U.L. from the Swedish Cancer Foundation, the Swedish Natural Science Research Council and the Granholms Foundation. M.D.R. was supported by a Muscular Dystrophy Association Postdoctoral Fellowship and J.C.M. was supported by an NIH Predoctoral training grant in biophysics.